MECHANICAL BEHAVIOUR OF JOINTS IN FSW: RESIDUAL STRESS, INHERENT STRAIN AND HEAT INPUT GENERATED BY FRICTION STIR WELDING

T. Terasaki, T. Akiyama
Department of Materials Science and Engineering, Kyushu Institute of Technology (Japan)
E-mail: terasaki@tobata.isc.kyutech.ac.jp

ABSTRACT

For ordinary arc welding processes such as MIG, welding deformation, residual stress and inherent strain are important factors to control the reliability of weldments. Friction stir welding (FSW) is a new welding method, especially for light metals. The distortion of FSW is reportedly small but reasons can not be determined in detail. This paper deals with thermal cycles and inherent strains which create both residual stresses and welding deformations, in order to make clear effective factors that lower apparent strains on FSW than on MIG. Inherent strains were measured by using the layer removal technique. Thermal cycles and maximum temperature rise were measured by type K thermocouples. It is concluded from experimental data that the main cause lowering apparent strain in FSW is the compressive load that makes tensile plastic strain in weldments. The second cause is that the heat input is smaller than in ordinary arc welding processes.

IIW Thesaurus keywords: *Friction stir welding; Welded joints; Residual stresses; Stress distribution; Stress; Strain; Temperature; Temperature distribution; Energy input; Measurement; Aluminium alloys; Hardness; Yield strength; Mechanical properties; Practical investigations; Reference lists.*

1 INTRODUCTION

Friction stir welding (FSW) was invented by Ole Midling *et al.* [1] and experimentally proven by Wayne Thomas *et al.* [2]. FSW has got into the spotlight as a new method of welding light metals, especially aluminum alloys. The benefits of FSW are as follows [3]:
– Low distortion (Low shrinkage),
– Excellent mechanical properties,
– No fumes.

The number of research papers on FSW increased in the past few years. Most of the papers deal with phenomena, processes and metallurgy. Only a few papers reported welding mechanical properties such as residual stresses and distortions [4]. It is described that the distortion by FSW is lower than that of arc welding such as MIG from experimental data. The following causes are given:
– The heat input of FSW is lower than that of MIG.
– The pressure mechanism of FSW causes the lower distortion.

The welding deformation and the residual stress are produced by the inherent strain that is generated by the combination of the welding heat input and the plate sizes [5]. The purpose of this paper is to investigate the causes of low distortion of FSW by the following experiments:

– the measurement of the inherent strain in the plate made by FSW,

– estimating the heat input of FSW by measuring thermal cycles.

Doc. IIW-1601-03 (ex-doc. III-1252-03/III-B-005-03) recommended for publication by Commission III “Resistance welding, solid state welding and allied joining processes”

2 EXPERIMENT

2.1 Welding procedures

FSW in this paper was performed at Kawasaki Heavy Industry in Japan by a machine that is able to control the compressive load given into the stir rod. The stir rod had a cylindrical shoulder of 15.5 mm in diameter and a probe of 5.5 mm in diameter. The base material plate (BM) was an extruded Al alloy 6063-T5 of 5 mm thickness h. Figure 1 shows a schematic diagram of FSW experiment. Two plates, 300 mm long and 60 mm wide, were butt welded by FSW as shown in Fig.1 (a). FSW was performed under two different welding speeds v of 3.3 mm/s and 10 mm/s. The compressive load F was also varied, 2250N and 3450N. The opposite sides of the butt joint were clamped tightly along the edges to hold the specimen immovable.

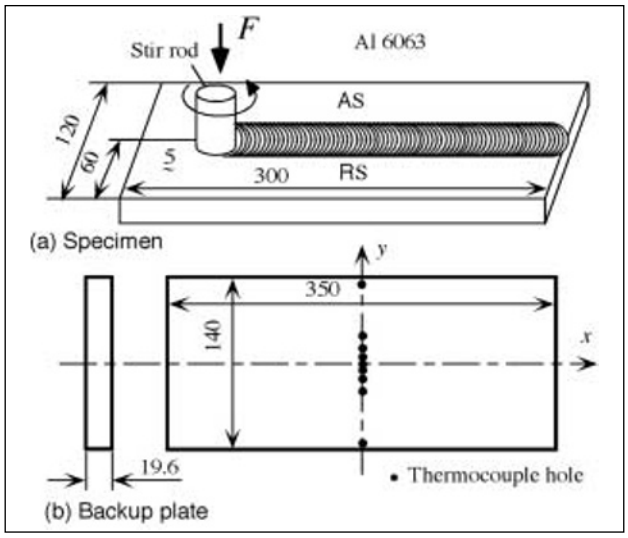

Fig. 1. Specimen of FSW and positions of thermocouple.

MIG welding was done under the following conditions: welding current *I*, the arc voltage *V* and the traveling speed *v* were 200A, 25V and 9.2 mm/s, respectively.

2.2 Measuring method of thermal cycle

The temperatures were measured at positions where the holes were drilled on the backup plate shown in Fig. 1(b). The type K thermocouples were inserted into the holes to contact with the specimen's back surface.

2.3 Measuring method of inherent strain

The specimens for measuring inherent strains were cut from both the advancing side (AS) in which the rotating direction of the stir rod agrees with the traveling direction of the rod and the opposite side named the retreating side (RS) [6]. A single strain gauge with a length of 0.5 mm was pasted on the opposite face of the welding bead of FSW as shown in Fig. 2. The gauge was coated with wax for preventing the permeation of humidity.

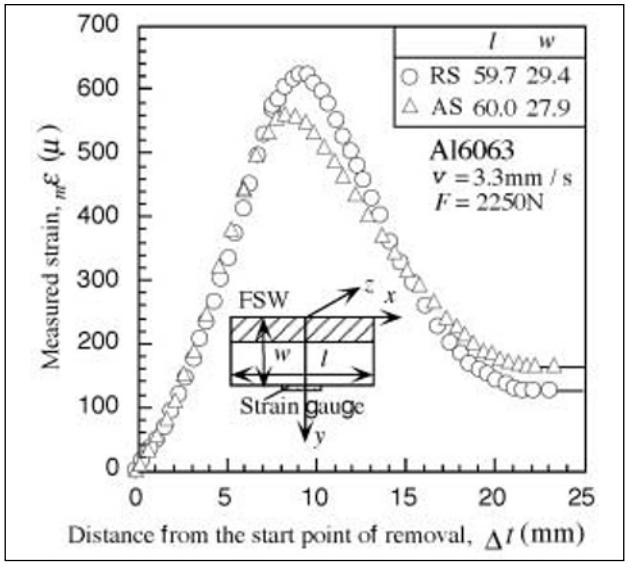

Fig. 2. Measured strain obtained by sequential layer removal technique.

A wet abrasive machine was used for sequential removal of thin layers. The inherent strains only exist in the vicinity of the weld metal [7]. The thin layers were removed from the bead side. The inherent strains were measured from experimentally measured strains in every thin removal layers within which the inherent strain was assumed to be constant [8-10].

2.4 Residual stress, hardness and yield strength

The residual stresses were determined by the stress-relaxation technique, which treats elastic strain released by cutting the specimen pasted strain gauges on it into thin pieces. Vickers hardness measurements were made on the center of the thickness of the cross section perpendicular to FSW direction, using a Vickers indenter with 4.9N load for 45 seconds. The 0.2% proof strengths of the weld metal and the base material were obtained from the piece of 5 mm thickness, 10 mm width and 40 mm length.

3 EXPERIMENTAL RESULTS AND DISCUSSION

3.1 Inherent strain

Figure 2 shows the relationship between the measured strain and the distance from the starting point of layer removal in the case of $F = 2250$N and $v = 3.3$ mm/s [11]. The symbols RS and AS mean the sides of the plate as shown in Fig. 1 (a). The cutting start position to separate the specimen of FSW into AS and RS was on the AS side, 2 mm away from the weld centerline. The work layer hardened by cutting was removed before the layer removal process in order to make the measured strain free from the effect of the strain introduced by cutting. The method for estimating inherent strains from measured strains was proposed by Fukuda [8] and Terasaki [12-13]. The theory developed in Ref. [8] is briefly explained. According to the elasticity theory, the cross section of the plate in Fig. 2, namely the *y-z* section, should be constantly plane when the length of the plate *l* is greater than twice the width *w*. Hence, the apparent strain in the direction of the *x*-axis is given as a linear function of *y* with unknown constants of *a* and *b*.

$$\varepsilon_x(y) = a + by \tag{1}$$

On the other hand, the apparent strain $\varepsilon_x(y)$ is the sum of the elastic strain $\varepsilon_{ex}(y)$ and the inherent strain $g_x(y)$.

$$\begin{aligned}\varepsilon_x(y) &= \varepsilon_{ex}(y) + g_x(y) \\ &= \sigma_x(y) / E(y) + g_x(y)\end{aligned} \tag{2}$$

where $E(y)$ is Young's modulus located at any point *y* in the material.

Equation (1) equals Equation (2), then

$$\begin{aligned}\sigma_x &= E(y)\{\varepsilon_x - g_x(y)\} \\ &= E(y)\{a + by - g_x(y)\}\end{aligned} \tag{3}$$

The unknown constants a and b are obtained from the following two equilibrium equations: (1) The resultant force in the x axial direction is zero. (2) The bending moment around the z-axis is zero.

$$a = \{\int_0^w E(y)g_x(y)dy \cdot \int_0^w E(y)y^2dz - \int_0^w E(y)g_x(y)ydy \cdot \int_0^w E(y)ydy\} / A \quad (4\text{-}1)$$

$$b = \{\int_0^w E(y)g_x(y)ydy \cdot \int_0^w E(y)dy - \int_0^w E(y)g_x(y)dy \cdot \int_0^w E(y)ydy\} / A \quad (4\text{-}2)$$

where

$$A = \int_0^w E(y)dy \cdot \int_0^w E(y)y^2dz - \{\int_0^w E(y)ydy\}^2 \quad (4\text{-}3)$$

The measured strains in Fig. 2 are given step by step after removing each layer sequentially from the initial specimen with the width w. The inherent strains in the removed layers are estimated from the measured strains by using Equations (3) and (4) as the inverse problem. This sequential layer removal technique only needs a small specimen containing the weld metal and the elastic part in which an inherent strain does not exist [9]. Figure 3 shows the distribution of inherent strain calculated from the measured strains shown in Fig. 2. The solid and open circle marks designate the inherent strain in the advancing side and the retreating side, respectively. The symmetry with the weld centerline of the inherent strain is shown in Fig. 3 by the absolute value of y in abscissa. The area where the inherent strain exists in AS is 25 mm and larger than the area of 23 mm in RS. The distribution of inherent strain is almost symmetric under condition of F = 2250 N and v = 3.3 mm/s. The area of $y \leq 7.7$ mm is the inner part of the shoulder radius of the stir rod and almost agrees with the area of plastic flow on the surface of the stir rod side.

The 0.2% proof stress in the weld metal was 86 MPa and Young's modulus for aluminum was 69 GPa [14], then the yield strain became 1246 μ. As the average value of inherent strains in the inner part of the shoulder was about -200 μ, so the inner part did not yield. The weld metal produced by arc welding generally yields and the residual stress is close to its yield strength [5], i.e. the value of inherent strain is the compressive yield strain [15]. Therefore, it seems that the compressive load causes as the characteristic of FSW.

As the inherent strain produced by shot peening is positive [13], it seems that the inherent strain in the inner part of the shoulder is obtained by adding the positive inherent strain produced by the downward force to the compressive yield strain caused by the welding thermal cycle. To check the above inference, changing the compressive load from 2250N to 3450N changed the inherent strain as shown in Fig.4. The inherent strain in the inner part of F = 3450N designated by the circle mark changes positive value from the negative value of F = 2250N designated by the triangle mark. It is clear from Fig. 3 that the inherent strain of FSW is made by adding two causes shown in the schematic diagram of Fig. 5; (1) the negative inherent value of the welding thermal cycle and (2) the positive inherent value of the compressive load.

Figure 6 shows the hardness H_V and the inherent strain under conditions of v = 10 mm/s and F = 3450N used as the field welding. The distribution of inherent strain does not exhibit a symmetry with the weld centerline. The area of inherent strain in AS is larger than that in RS in the same manner as shown in Fig. 3.

3.2 Residual stress distribution

The residual stresses obtained by the stress-relaxation technique were compared with those estimated by the combination of the inherent strains and the finite element method (FEM). The inherent strain of FSW is considered to be uniform along the welding line, namely the x-axis, then the inherent strain in the x-direction g_x and that in the y-direction g_y, respectively are the only y function. When introducing g_y into the specimen, for the example shown in Fig. 1 (a), the transverse shrinkage is produced as a result of the non-restraint in the y-direction after FSW, but the residual stress is not generated. After all, the residual stress is produced only by g_x.

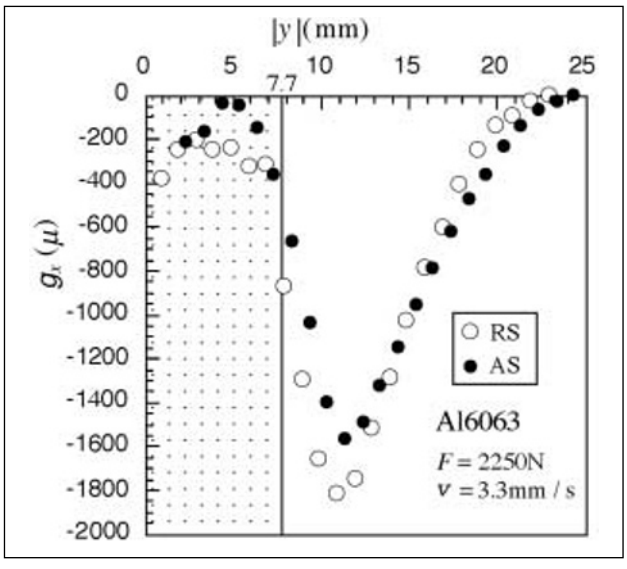

Fig. 3. Distribution of inherent strain.

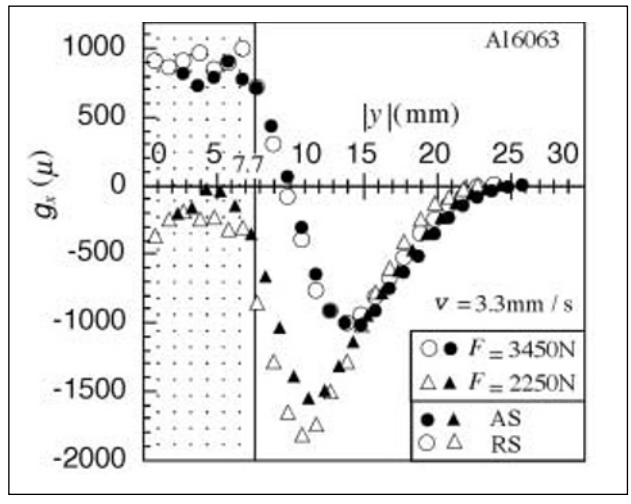

Fig. 4. Effect of compressive load on inherent strains.

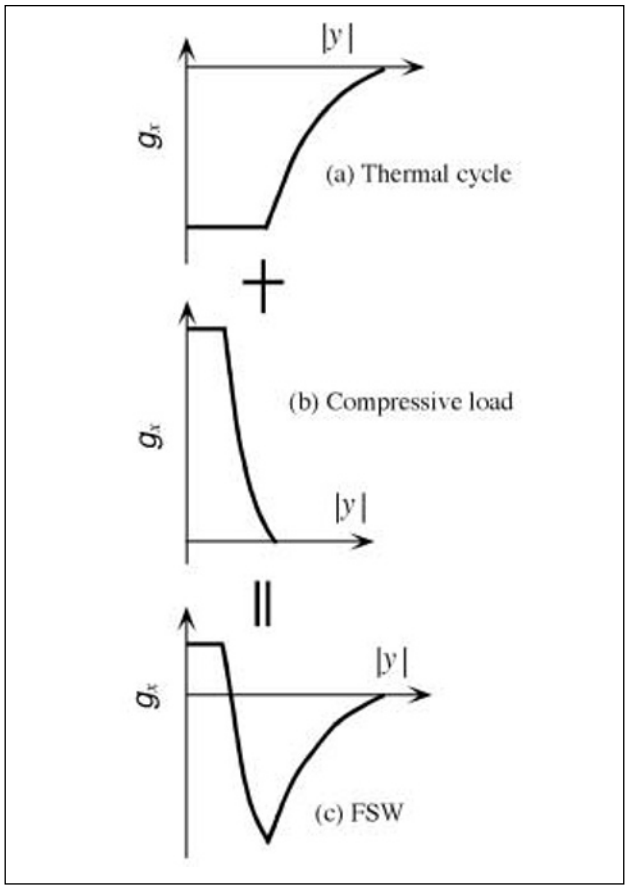

Fig. 5. Cause of inherent strain generated by FSW.

Figure 7 shows the residual stress of the stress relaxation designated by the solid triangle and that of the inherent strain designated by the open circle in the case of F = 3450N and v = 10 mm / s. The values of the residual stress on the bead do not agree with each other, but those on other places agree approximately. The residual stress changes sharply into small value within the bead, which is induced by the compressive load mentioned above as a FSW feature.

3.3 Thermal cycle

The inherent strain in the welded joint is produced by the temperature rise and the restraint. We used the clamped

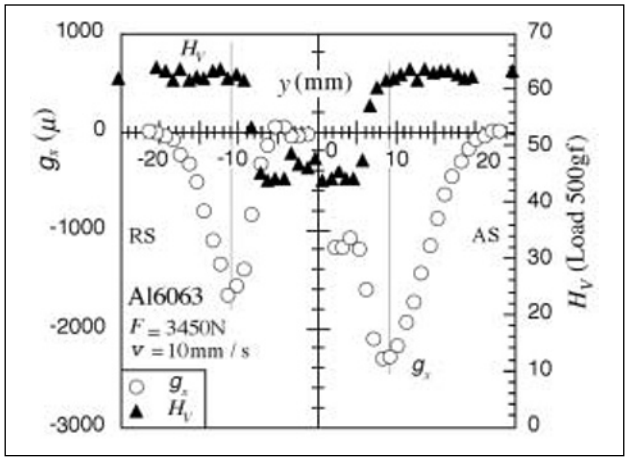

Fig. 6. Relation between inherent strain and hardness distributions.

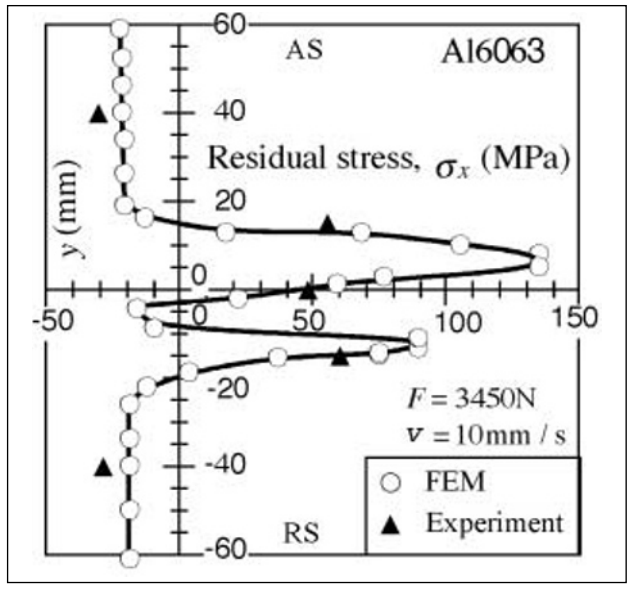

Fig. 7. Comparison between experimental data and numerical results calculated from inherent strains of residual stress.

bar model shown in Fig. 8 which is useful for estimating the distribution of inherent strain [5], [15]. The 0.2% proof strength of base material Al6063 is 192 MPa, then the yield strain of BM is 2840 μ. The linear expansion coefficient α of aluminum is 2.4×10^{-5} ($^oC^{-1}$) [14]. The boundary line y_p of inherent strain in the y-direction is the position at which the maximum temperature rise T_p is given by the following equation:

$$T_p = \varepsilon_y / \alpha = 284 \times 10^{-5} / 2.4 \times 10^{-5} = 118^oC \quad (5)$$

Where the maximum temperature rise is greater than twice T_p, the value of inherent strain is the compressive yield strain and constant [5]. In practice, the value changes from the compressive yield strain to another value by causing hardening of the steel and fading the age hardening in the aluminum alloy of heat treatment. In the welding mechanical field, the important rises of maximum temperature are T_p and 2 T_p.

The figures in Fig. 9 show the value of the temperature rise generated by FSW. The dotted circle is the inside of the stir rod shoulder diameter. Figure 9(a) shows the isothermal temperature rise in the case of v = 10 mm/s and F = 3450N. The abscissa X is the distance from the position of the stir rod and taken in the opposite direction of welding. As the temperature rise at the position opposite to the stir rod on the section of X = 0 is 0°C, the free expansion on the section of X = 0 does not exist. Figure 9(b) shows the isothermal temperature rise

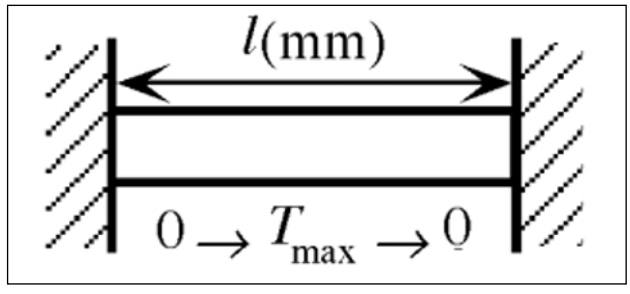

Fig. 8. Clamped bar model.

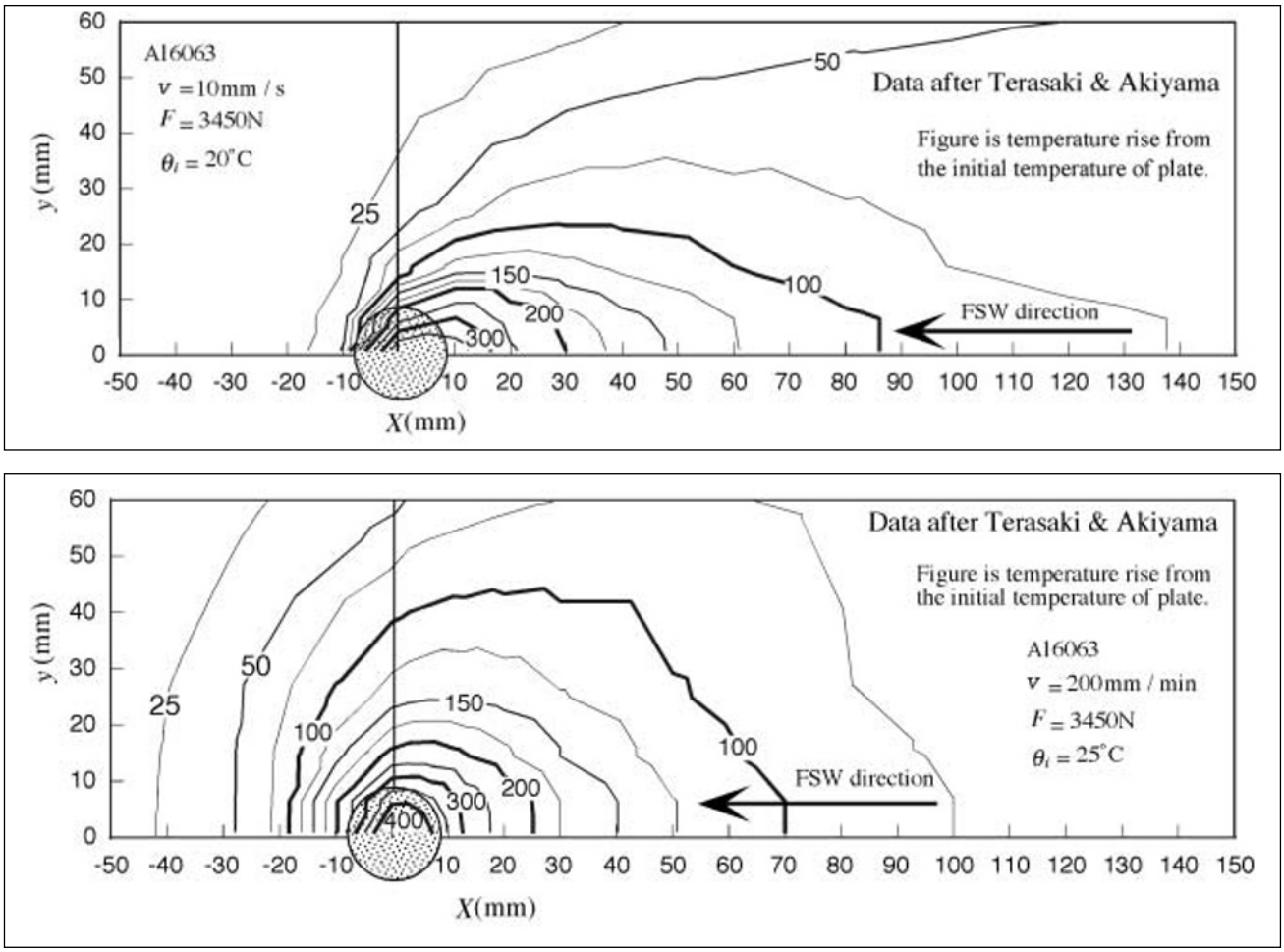

Fig. 9. Distribution of temperature rise generated by FSW: (a) in case of travel speed being 10mm/s, (b) in case of travel speed being 3.3 mm/s.

in the case of v = 3.3 mm/s and F = 3450N. As the temperature rise at the position opposite to the stir rod on the section of X = 0 is about 50°C, the free expansion on the section of X = 0 is about 50 α.

3.4 Inherent strain vs. the maximum temperature rise

Figure 10(a) shows the distribution of the inherent strain and the maximum temperature rise, respectively, in the case of F = 3450N and v = 10 mm/s. The maximum temperature rise becomes 120°C at the boundary line of inherent strain, which is 21 mm away from the centerline. From Fig.10 (a) and Eq. (5) mentioned above in section 3.3, the experimental value 120°C agrees approximately with the predicted value 118°C. Figure 10(b) shows the distribution of the inherent strain and the maximum temperature rise, respectively, in the case of F = 3450N and v = 3.3 mm/s. The boundary line of inherent strain is at 23.5 mm and the maximum temperature

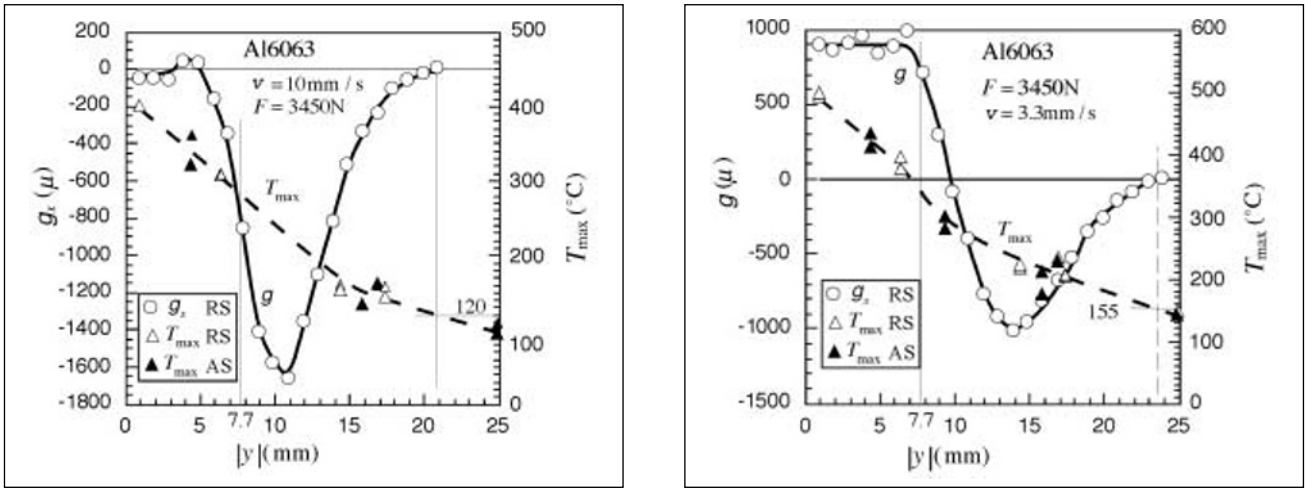

(a) in case of travel speed being 10 mm/s **(b) in case of travel speed being 3.3 mm/s**

Fig. 10. Relation between maximum temperature rise and inherent strain distribution.

rise becomes 155°C. The experimental value 155°C agrees approximately with the predicted value 168°C calculated by adding the predicted value 118°C of Eq. (5) to the free expansion temperature 50°C obtained from Figure 9(b) and section 3.3. As a conclusion, the boundary line of inherent strain produced by FSW is estimated by Eq. (5) obtained from the clamped bar model, which is useful in the arc and the laser welding of steel [15].

3.5 Distribution of inherent strain produced by FSW

Figure 11 shows the hardness and the inherent strain distribution, respectively, in the case of F = 3450N and v = 3.3 mm/s. The hardness distribution is almost symmetrical with the weld centerline. By investigating the hardness and the inherent strain distributions, it is shown that the position at which the hardness starts to decrease almost agrees with the position where the inherent strain shows a minimum value as shown in Fig. 6 and Fig. 11.

Summarizing section 3.1 to section 3.5, the characteristic points in the inherent strain distribution obtained from FSW Al6063 joints are shown in Fig.12. y_0 designates the compressive load area by the stir rod and the plastic flow. y_H designates the position at which hardness starts to be softened by the FSW temperature that anneals the age hardening in the aluminum alloy. y_p designates the area of inherent strain predicted by Eq. (5).

3.6 FSW heat input

It is important to estimate the heat input generated by FSW to solve many problems in the welding field. However, an equation to estimate the heat input of FSW does not exist. The equation for heat input is investigated from experimental data on thermal cycles for estimating the characteristic points of the inherent strain and the hardness. The microstructural changes caused by FSW in aluminum alloy Al6063-T5 were studied in

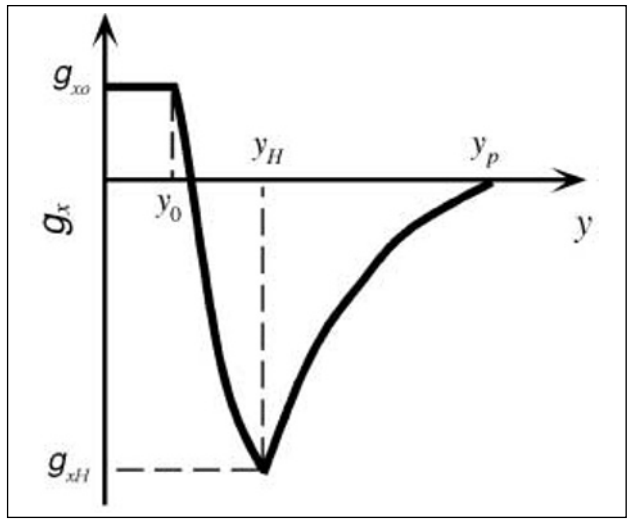

Fig. 12. Special points of inherent strain distribution generated by FSW.

detail by Sato [16]. He observed the following: the minimum hardness due to softening appears in the region where the temperature is over 350°C. The temperature just on the hardness decreasing point, namely y_H in Fig. 12, is 227°C.

Figure 13 shows the maximum temperature and the hardness obtained by FSW in case of F = 3450N and v = 3.3 mm/s. The temperatures at both points where the minimum hardness value appears and the hardness starts to decrease are 350°C and 240°C, respectively. The temperature of the minimum hardness 350°C agrees with Sato's result. The temperature difference at y_H is 13°C. Then it is possible to estimate the FSW heat input from experimental data, i.e. the distance y_v from the weld centerline to the boundary line of minimum hardness due to softening, the maximum temperature 350°C (Θ_V), and the initial temperature of base material Θ_i.

First, we investigated the equation dealing with the maximum temperature rise T_{max} (= Θ_{max}-Θ_i), which is widely needed in the mechanical problem. Figure 14 shows experimental data represented by open circles and the calculated results represented by solid curves obtained

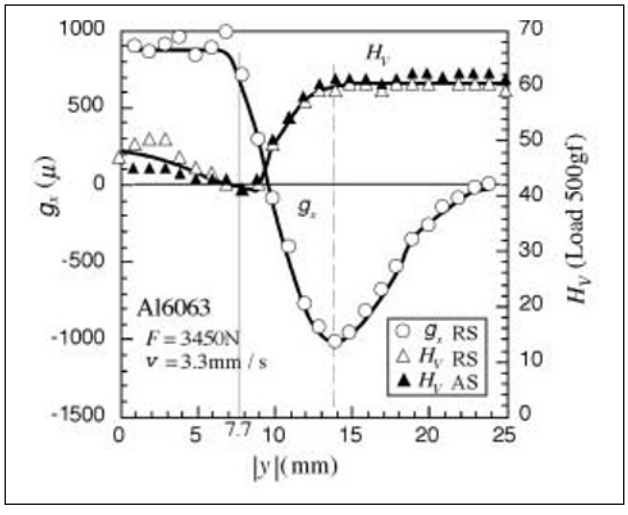

Fig. 11. Relation between inherent strain and hardness distributions.

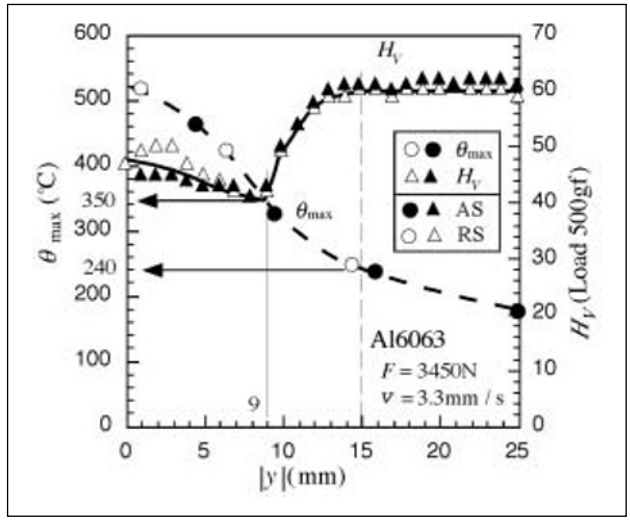

Fig. 13. Relation between maximum temperature and hardness.

under conditions of F = 3450N, v = 3.3 mm/s and Θ_i = 25°C. The maximum temperature rise T_V (= Θ_V - Θ_i) becomes 325°C. From experimental data (open circles), the position of temperature 325°C (y_V) becomes 8 mm as shown in Fig.14. In case of instantaneous plane source, the maximum temperature rise T_{max} is given by the following equation [5]:

$$T_{\max} = 0.242 Q_{net} / c\,\rho h y \tag{6}$$

where

c is the specific heat J/g°C

ρ is the density (g / mm^3)

Q_{net} is net heat input (J/mm).

Then the heat input is given by the following

$$Q_{net} = c\,\rho h y_v\,(\theta_v - \theta_i)/0.242 \tag{7}$$

The material constants of aluminum are c = 0.9 J/g°C and ρ = 0.0027 g/mm^3.

The thin solid curve in Fig.14 is calculated by Eqs. (6) and (7) using y_V = 8 mm, θ_V = 350°C and θ_i = 25°C. By comparing experimental data with the thin solid curve, Eq. (6) on the maximum temperature rise based on the instantaneous plane source is not useful for Al alloys, but effective for steel [5], the main cause for this being that the thermal diffusivity k of aluminum being 8 times that of steel [14], then the effect of moving the heat source influences the rise of temperature [17]. In the case of a moving line source, the rise of temperature T is given by Rosenthal [18] as follows:

$$T = (q / 2\pi\lambda h)\exp(vX/2k)\cdot K_0(\sqrt{(vX/2k)^2 + (vy/2k)^2}) \tag{8}$$

$$T_{max} = (q / 2\pi\lambda h)\exp(vX_M/2k)\cdot K_0(\sqrt{(vX_M/2k)^2 + (vy/2k)^2}) \tag{9}$$

where X_M satisfies the following equation:

$$X_M / \sqrt{X_M^2 + y^2} = K_0\,(v\sqrt{X_M^2 + y^2}\,/\,2k)\,/\,K_1\,(v\sqrt{X_M^2 + y^2}\,/\,2k) \tag{10}$$

K_1 is the modified Bessel function of first order, second kind.

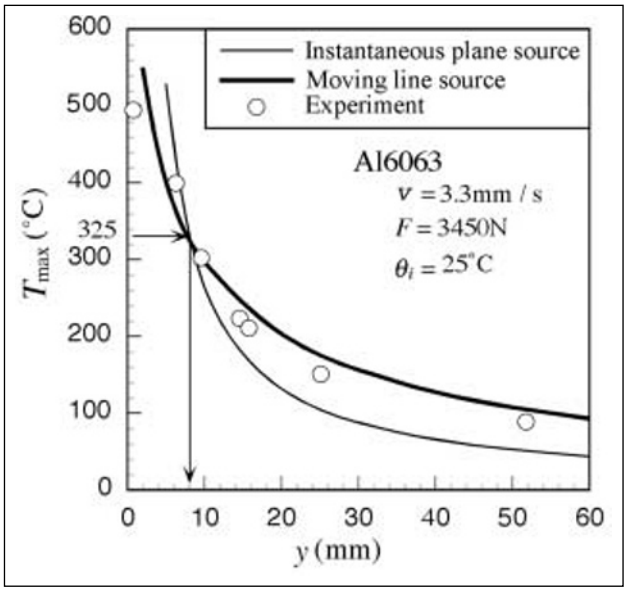

Fig. 14. Maximum temperature rises obtained by experiment and heat conduction theory.

The heat input per unit time is given by substituting the data on the temperature θ_v at y_V and the initial temperature θ_i into Eq. (9):

$$q = 2\pi\lambda h\,(\theta_v - \theta_i)\cdot\exp(-vX_v/2k)\,/\,K_0(\sqrt{(vX_v/2k)^2 + (vy_v/2k)^2}) \tag{11}$$

where X_V satisfies the following equation:

$$X_v / \sqrt{X_v^2 + y_v^2} = K_0\,(v\sqrt{X_v^2 + y_v^2}\,/\,2k)\,/\,K_1\,(v\sqrt{X_v^2 + y_v^2}\,/\,2k) \tag{12}$$

The thick line in Fig.14 is calculated by Eq. (9) and (11) with the values y_V = 8 and T_V = 325°C using λ = 0.19 J/s mm °C for an aluminum alloy [14]. The experimental data (open circles) almost agree with the thick line.

Table 1 shows experimental conditions of all data, the softening position of temperature y_V and heat inputs calculated by Eq. (9) and (11). The heat input per unit weld length Q_{net} (J/mm) is given by dividing the heat input per unit time by the welding speed. Though the experimental conditions of FSW are same in specimens 3 and 4, data y_V have a slight difference. The heat inputs Q_{net} for specimens 3 and 4 are 323 and 341 J/mm, respectively. The difference is about 6%. From Table 1 the heat input Q_{net} is considerably affected by the welding speed, but not so much by the compressive load.

3.7 MIG welding and FSW

As the thermal efficiency obtained by MIG welding of aluminum is not clear, we used the thermal efficiency of steel η = 0.7 to calculate the net heat input Q_{net} in the welded plate. The heat input Q_{net} is 382 J/mm calculated by the equation $Q_{net} = \eta IV / v$. The FSW heat input shown in Table 1 exists in the range of 148 J/ mm to 341 J/mm, then the FSW heat input is smaller than that of MIG Welding. Figure 15 shows the inherent strain distribution obtained by MIG welding and that by FSW of 323 J/mm shown in Fig. 4. The value of inherent strain inside about 8 mm corresponding to the weld metal shows a striking difference between FSW and MIG welding. This cause is the compressive load used in FSW. The influence of the heat input of MIG being larger than that of FSW appears the value of y_p. As the difference of the heat input 382J/mm and 323 J/mm by MIG and FSW, respectively, is small, these y_p values do not differ extremely. In the case of the heat input 164 J/mm in the specimen 6 with F = 3450N and v = 10 mm/s, the value of y_p shown in Fig. 6 is smaller than that of MIG in Fig. 15. The low distortion and low residual stress generated by FSW are due to the following two causes:

Table 1. Heat input of FSW.

Specimen	v (mm / s)	F (N)	y_V (mm)	q (J / s)	Q_{net} (J / mm)
1	3.33	2250	9	1135	341
2	3.33	2250	8	1075	323
3	3.33	3450	8	1075	323
4	3.33	3450	9	1135	341
5	10.0	2850	5	1477	148
6	10.0	3450	6	1637	164
7	10.0	3450	6.5	1717	172

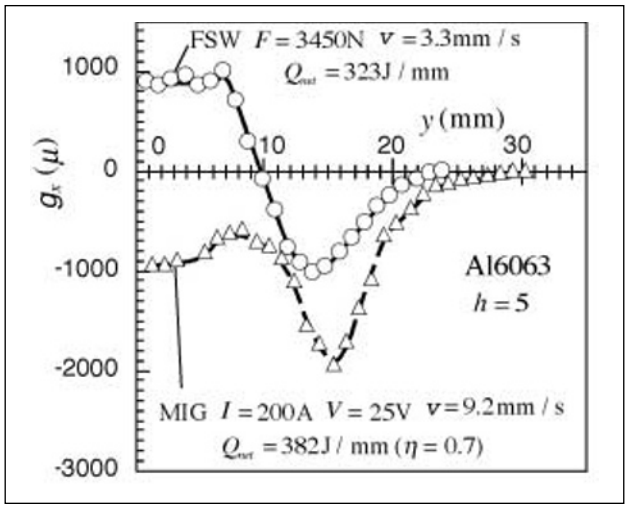

Fig. 15. Comparison of inherent strain distributions caused by MIG and FSW.

1 The compressive load makes the positive value or the small negative value of inherent strain at the weld metal.

2 The low heat input makes the small value of y_p indicating the existence of inherent strain.

4 CONCLUSIONS

The inherent strain and the maximum temperature produced by FSW were investigated. The main results were as follows:

1 The inherent strain distribution is affected by the compressive load of FSW, and the inherent strain value is given by adding the positive inherent value by compressive load to the negative inherent value of welding thermal cycle as shown in Fig. 5.

2 The residual stress distribution estimated by the inherent strain and FEM almost agrees with that obtained by the stress-relaxation technique.

3 The characteristic points of inherent strain distribution shown in Fig.12 are the following three points: the boundary position subjected to the compressive load by the stir rod, the position where the hardness starts to decrease itself by softening based on welding heat and the existence point of inherent strain predicted by the clamped bar model.

4 The heat input of Al6063 plates welded by FSW is estimated by the temperature and the position of minimum hardness, the initial temperature of base material and the equation predicting the maximum temperature rise of the moving line source.

5 Comparison between the distribution of inherent strain of FSW and that of MIG show that the causes of low distortion of FSW are the compressive load and the low heat input.

REFERENCES

1. Midling, O.T., Morley, E.J., Sandvik, A., Friction stir welding, European Patent Application 959 078 88.2.

2. Thomas, W.M., Nicholas, E.D., Needham, J.G., Murch, M.G., Temple-Smith, P., Dawes, C.J., Improvements relating to friction welding, European Patent Specification 0615 480 B1.

3. www.twi.co.uk/bestprac/datashts/fswproc.html.

4. Chao, Y.J. and Qi, X., Heat Transfer and Thermo-Mechanical Analysis of Friction Stir Joining of AA6061-T6 Plates, 1st International Symposium on Friction Stir Welding, 14-16, June, 1999, USA.

5. Watanabe, M. and Satoh, K., Welding Strength and Application, (1965), Asakura.

6. Thomas, W. M., Threadgill, P.L. and Nicholas, E.D., Feasibility of friction stir welding steel, Science and Technology of Welding and Joining, 4 (1999), 365-372.

7. Fukuda, K., General Theory of Measuring Residual Stresses and New Measuring Method of 3-Dimensional Residual Stresses, (in Japanese) 1979, Ph. D. thesis of Osaka University.

8. Fukuda, K., Kim, Y., Akiyama, T. and Terasaki, T., Method for Estimating Residual Stress Produced in Sprayed Coating and Substrate by means of the Concept of Inherent Strain, (in Japanese), Thermal Spray, 27 (1990), 124-131.

9. Terasaki T., Akiyama, T. and Ishimura, T., New Method for Estimating Residual Stresses in Pipe Made by Surfacing Weld, ASME J. Eng. Ind., 117 (1995), 365-371.

10. Chen, J., Terasaki, T., Akiyama, T. and Kishitake, K., New Concept of Equivalent Inherent Strain for Measuring Axisymmetric Residual Stresses, ASME J. Manuf. Sci. and Eng., 122 (2000), 304-309.

11. Terasaki, T., Yamasaki, M. and Akiyama, T., Cause of Residual Stress Produced by Friction Stir Welding, (in Japanese), Joining and Materials Processing for Light Structures MP-267-2000 (2000), Japan Welding Society.

12. Terasaki, T., Akiyama, T. and Yoshimura N., A Study on Residual Stress in Evaporation Coating Film, (in Japanese), Jpn. Soc. Mech. Eng., 59 A (1993), 2694-2701.

13. Terasaki, T., Chen, J., Akiyama, T. and Kishitake, K., Non-Destructive Method for Estimating Residual Stress Distributin in Component due to Shot Peening, JSME International Jour., Series A, 42 (1999), 216-223.

14. Aluminum handbook, The Japan Institute of Light Metals (1994).

15. Terasaki, T. and Fukuya, M., Distribution of Inherent Strain Generated in Butt Joint, (in Japanese), Jpn. Soc. Mech. Eng., 66 A (2000), 1233-1238.

16. Sato, Y., Kokawa, H., Enomoto, M. and Jogan, S., Microstructural Evolution of 6063 Aluminum during Friction Stir Welding, Metal. Mater. Trans. A, 30 (1999), 2429-2437.

17. Satoh, K., A Note On Heat Conduction By Moving Heat Source (in Japanese), J. of Japan Welding Society, 36 (1967), 154-159.

18. Rosenthal, D., The theory of Moving Sources of Heat and Its Application to Metal Treatments, ASME, 68 (1946), 849-866.

19. Wells, A.A., Heat Flow in Welding, W.J., 31 (1952), 263s-267s.

20. Terasaki, T., Matsuyama, K. and Kamikihara, H., Experiment and Predictive Equation of Heat Input Generated in Plate by Thermal Cutting Process, IIW(2000), IE-314-00.